RSC Advances

PAPER

View Article Online
View Journal | View Issue

Cite this: *RSC Adv.*, 2022, **12**, 24192

Benzodioxole grafted spirooxindole pyrrolidinyl derivatives: synthesis, characterization, molecular docking and anti-diabetic activity†

Narayanasamy Nivetha,[a] Reshma Mary Martiz,[b] Shashank M. Patil,[b] Ramith Ramu,[b] Swamy Sreenivasa[c] and Sivan Velmathi *[a]

Received 19th July 2022
Accepted 11th August 2022

DOI: 10.1039/d2ra04452h

rsc.li/rsc-advances

A highly stereoselective, three-component method has been developed to synthesize pyrrolidine and pyrrolizidine containing spirooxindole derivatives. The interaction between the dipolarophile α,β-unsaturated carbonyl compounds and the dipole azomethine ylide formed *in situ* by the reaction of 1,2-dicarbonyl compounds and secondary amino acids is referred to as the 1,3-dipolar cycloaddition reaction. The reaction conditions were optimized to achieve excellent stereo- and regioselectivity. Shorter reaction time, simple work-up and excellent yields are the salient features of the present approach. Various spectroscopic methods and single crystal X-ray diffraction examinations of one example of compound **6i** validated the stereochemistry of the expected products. The anti-diabetic activity of the newly synthesized spirooxindole derivatives was tested against the α-glucosidase and α-amylase enzymes. Compound **6i** was found to exhibit potent inhibition activity against α-glucosidase and α-amylase enzymes which is further evidenced by molecular docking studies.

Introduction

Synthetic organic chemistry has been pursuing the efficient transformation of basic starting materials into highly functionalized complex products that combine environmental and economic benefits. In this context, multicomponent reactions (MCRs) have emerged as a particularly effective synthetic tool for achieving this aim. The field of 1,3-dipolar cycloaddition reactions has recently exploded in popularity for the multicomponent synthesis of spirocyclic motifs. Spiro compounds are ubiquitously essential core units of many natural or synthesised substrates, and they include a wide range of organic molecules of chemical, industrial, and medicinal importance.[1,2]

Spirooxindoles are a unique family of heterocyclic scaffolds since they have been used in drug development as structural and adjacent units at the perimeter of substrates. Because of their unusual three-dimensional structural characteristics, spiro compounds are predicted to bind adequately with protein active sites more easily than flat aromatic ring systems. The inclusion of the oxindole core and additional heterocyclic moieties (typically fused at the oxindole's C-3 position) makes these motifs attractive drug development targets.[3] Among them, the spiro-pyrrolidinyl oxindoles were utilized as promising synthetic intermediates[4] and exhibited notable biological activities, including anti-diabetic,[5] antifungal[6] anti-inflammatory, anti-tumour,[7] anti-tubercular, antimalarial,[8] acetylcholinesterase (AChE), and antiviral[9] inhibition properties. For instance, Spirotryprostatin A and B are inhibitors of microtubule assembly and also display antibiotic as well as anti-cancer properties.[10] Further, pteropodine works as a positive modulator of 5-HT2 and muscarinic M2 receptors (Fig. 1).[11] Spirooxindole pyrrolidinyl frameworks consisting of Horsifiline and Coerulescine are employed as an analgesic and local anesthetic, respectively.

Through C–C and C–X bond forms, 1,3-dipolar cycloadditions[12] play a crucial role in the building of complex heterocyclic motifs. The multicomponent 1,3-dipolar cycloaddition of azomethine ylides generated *in situ* from the decarboxylative condensation of 1,2-dicarbonyl compounds and α-amino acids to exocyclic olefinic dipolarophiles have attracted a great deal of attention.[13] Through two C–C and one C–N bond-forming processes, as well as the development of four new conterminous stereocentres in a single transformation, this sort of one-pot three-component technique allows the construction of architecturally intriguing spirocyclic hybrids.[14]

MCRs (multicomponent reactions) are environmentally friendly reactions in which three or more reactants combine to produce complex products with high atom economy by

[a]*Organic and Polymer Synthesis Laboratory, Department of Chemistry, National Institute of Technology, Tiruchirappalli, 620 015, Tamil Nadu, India. E-mail: velmathis@nitt.edu*

[b]*Department of Biotechnology and Bioinformatics, School of Life Sciences, JSS Academy of Higher Education and Research, Mysuru, 570 015, Karnataka, India*

[c]*Department of Chemistry, University College of Science, Tumkur University, Tumkur, 572 103, Karnataka, India*

† Electronic supplementary information (ESI) available. CCDC 2143927. For ESI and crystallographic data in CIF or other electronic format see https://doi.org/10.1039/d2ra04452h

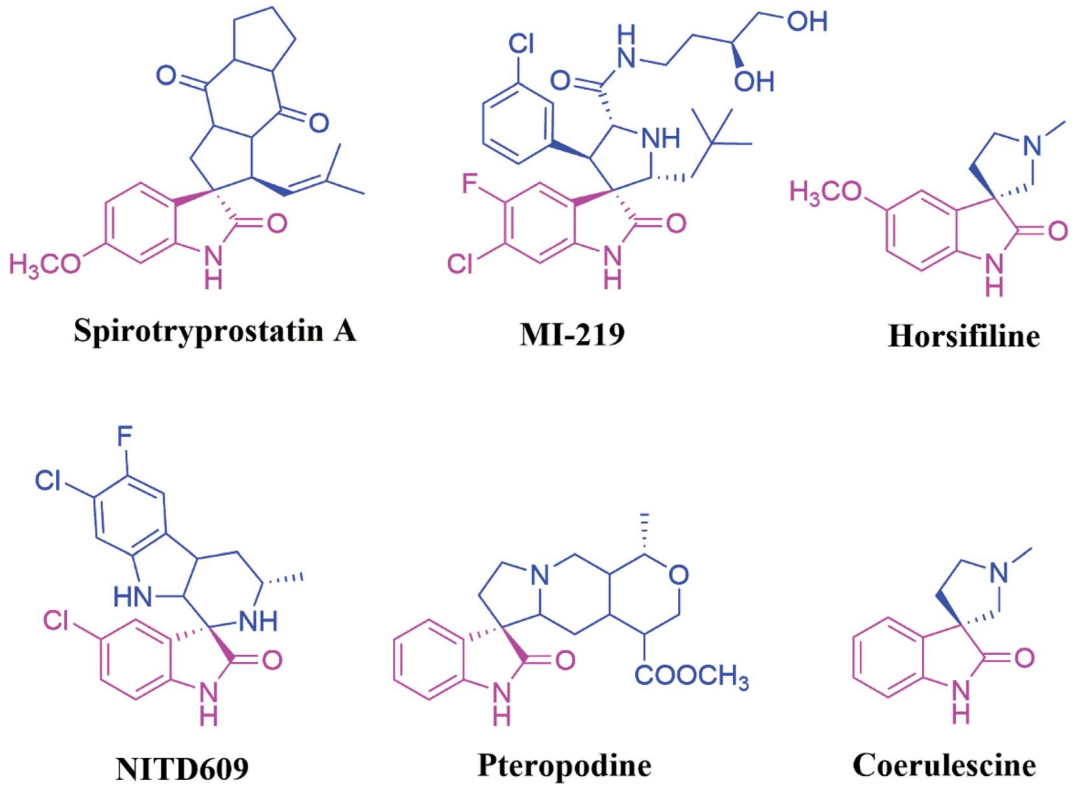

Fig. 1 Spirooxindole core consisting of some bioactive compounds.

combining all of the starting ingredients. In organic synthesis and drug discovery programs, MCRs are cost-effective, time-saving, and provide the required product in high yield under simple and moderate reaction conditions.[15,16] These synthetic procedures provide for faster access to a more robust platform for building structurally complicated molecule libraries.[17]

Diabetes is one of the worldwide prevalent epidemic diseases. Globally, around 463 million people were living with diabetes as of 2019, whereas it is estimated that by 2045 the count will be raised to 700 million, approximately.[18] Increment of blood glucose levels, a common cause of uncontrolled diabetes, may, on the extension of time lead to serious consequences, like liver damage, strokes, peripheral nephropathy, coronary heart disease, nephropathy and retinopathy.[19] Diverse digestive enzymes incorporated in starch hydrolysis are present in the small intestine and oral cavity.[20,21] Among them, α-glucosidase and α-amylase are essential enzymes in the digestion of glycogen and starch[22] and play significant roles in controlling the postprandial glucose concentration.[23] Thus, inhibition of either or both α-glucosidase and α-amylase is an efficacious way to diminish postprandial glycaemia. The inhibitory activity of these enzymes can impede the transport of carbs into the circulation, reducing the postprandial rise in blood glucose following a mixed carbohydrate meal, and hence can be an important approach in the management of type 2 diabetes.[24]

Anti-hyperglycemic medicines like acarbose, voglibose, and miglitol are used to treat type 2 diabetes because they block α-glucosidase or α-amylase and are effective at controlling post-prandial blood glucose levels. However, the negative side effects and expensive cost have limited their use.[25] Because diabetes affects about 5% of the global population, its management without side effects remains a challenge for the medical community. As a result, research into agents for this purpose has grown in importance, and researchers are competing to find new effective and safe therapeutic agents for diabetes treatment.[26–31]

In continuation of our interest towards the synthesis of potent bioactive spirocyclic hybrids by developing biocompatible methodologies,[32] we report herein the regio- and stereoselective three-component synthesis of a novel class of spirooxindole pyrrolidine and pyrrolizidine moieties. The synthesis was accomplished by 1,3-dipolar cycloaddition of benzodioxole chalcones to azomethine ylides generated *in situ* from isatin and sarcosine/L-proline. Further, the synthesized compounds were subjected to anti-diabetic activity against α-glucosidase and α-amylase enzymes.

Results and discussion

Chemistry

In the presence of appropriate reaction conditions, a one-pot, three-component, 1,3-dipolar cycloaddition process combining the dipolarophiles as benzodioxole chalcones and the dipole as azomethine ylide was used to synthesise desirable spirooxindole derivatives.

The benzodioxole chalcones (**1a–l**) were prepared according to the literature procedure[33] with slight modification. Herein, the reaction involves Claisen–Schmidt condensation of 3,4-(methylenedioxy)acetophenone and different substituted benzaldehydes in alkaline medium (10 percent KOH) at room temperature, and were further purified by recrystallization from ethanol in good yield.

We investigated the reaction conditions for the synthesis of spirooxindole pyrrolidine and pyrrolizidine derivatives through the 1,3-dipolar cycloaddition reaction using *in situ* generated azomethine ylide, which results in the formation of three new bonds, one spirocyclic quaternary carbon, and four stereocenters in a single step using these benzodioxole chalcones as dipolarophiles.

An equimolar quantity of dipolarophile (**1a**), isatin (**2**) and sarcosine (**3**) were taken as a model substrate for examining the synthesis of benzodioxole substituted spirooxindole pyrrolidine (**5a**) as shown in Table 1.

Polar aprotic solvents including dimethylformamide (DMF), acetonitrile, dichloromethane (DCM) and 1,4-dioxane and non-polar aprotic solvent like toluene produced desired product in lesser yield, due to the reason that the starting materials were sparingly soluble in these solvents even at the reflux temperature and prolonged time (Table 1, entry 1–6). We further investigated with various polar protic solvents such as methanol, ethanol, water and methanol:water systems to monitor the progress of the reaction (Table 1, entry 7–11). The reaction proceeded well in the case of methanol as the solvent to furnish the desired product in good yield and shorter time (Table 1, entry 7). Besides, by increasing or decreasing the mole ratio of amino acids and 1,2-dicarbonyl compound as well as the reaction temperature, there is no significant enhancement in the efficiency and yield of the reaction.

Consequently, unstabilized azomethine ylides were formed *in situ* by the decarboxylative condensation of isatin (**2**) and sarcosine (**3**), which rapidly reacted with the dipolarophiles (**1a–l**) under reflux in methanol by 1,3-dipolar cycloaddition reaction to afford novel spirooxindole pyrrolidine derivatives (**5a–l**) in excellent yields (Table 2).

This cycloaddition reaction is stereo- and regioselective, with the β-carbon of the α,β-unsaturated compounds of the dipolarophile adding to electron-rich carbon of the dipole. The successful synthesis of the spirooxindole pyrrolidine (**5a–l**) and pyrrolizidine (**6a–l**) derivatives were established by spectroscopic and crystallographic studies. Scrutiny of all spectral data confirmed the formation of the spirooxindole derivatives obtained from the benzodioxole chalcones as dipolarophiles.

The molecular structure of the newly synthesized spirooxindole pyrrolidine derivatives **5a–l** was elucidated by FT-IR, proton NMR, carbon NMR and High-resolution Mass Spectrometry (HR-MS). The FT-IR spectrum of the compound **5c** showed oxindole –NH stretching at 3348 cm^{-1}, benzodioxole $-OCH_2O-$ exhibited characteristic stretching vibration at 2916 cm^{-1} and C=O stretching at 1720 and 1659 cm^{-1} for oxindole and benzodioxole carbonyls, respectively.

In the ^1H NMR spectrum, compound **5c** exhibited a singlet at δ 2.06 for pyrrolidine $N-CH_3$ protons. The doublet for the methylene protons (H-5) appeared at δ 3.39 and the methine

Table 1 Optimization of the reaction conditions for the synthesis of spirooxindole derivatives[a]

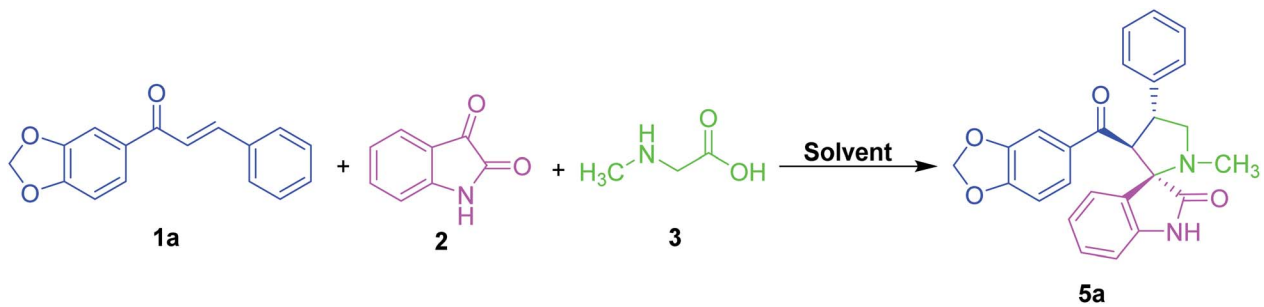

Entry	Solvent	Temperature (°C)	Time (h)	Yield[b] (%)
1	DMF	120	8.5	50
2	Acetonitrile	85	5	65
3	DCM	40	6	55
4	1,4-Dioxane	90	4	70
5	Methanol: 1,4-Dioxane (1 : 1)	80	6.5	74
6	Toluene	100	10	45
7	**Methanol**	**67**	**1.5**	**80**
8	Methanol	RT[c]	12	NR[d]
9	Ethanol	80	1.5	76
10	Water	90	10	NR[d]
11	Methanol: Water (1 : 1)	75	5	60

[a] All reactions were carried out with **1a** (1 mmol), **2** (1 mmol) and **3** (1 mmol). [b] Isolated yields. [c] RT = room temperature. [d] NR = no reaction. The entry in bold indicates optimal condition.

Table 2 Substrate scope for the stereo- and regioselective synthesis of spirooxindole pyrrolidine derivatives[a,b]

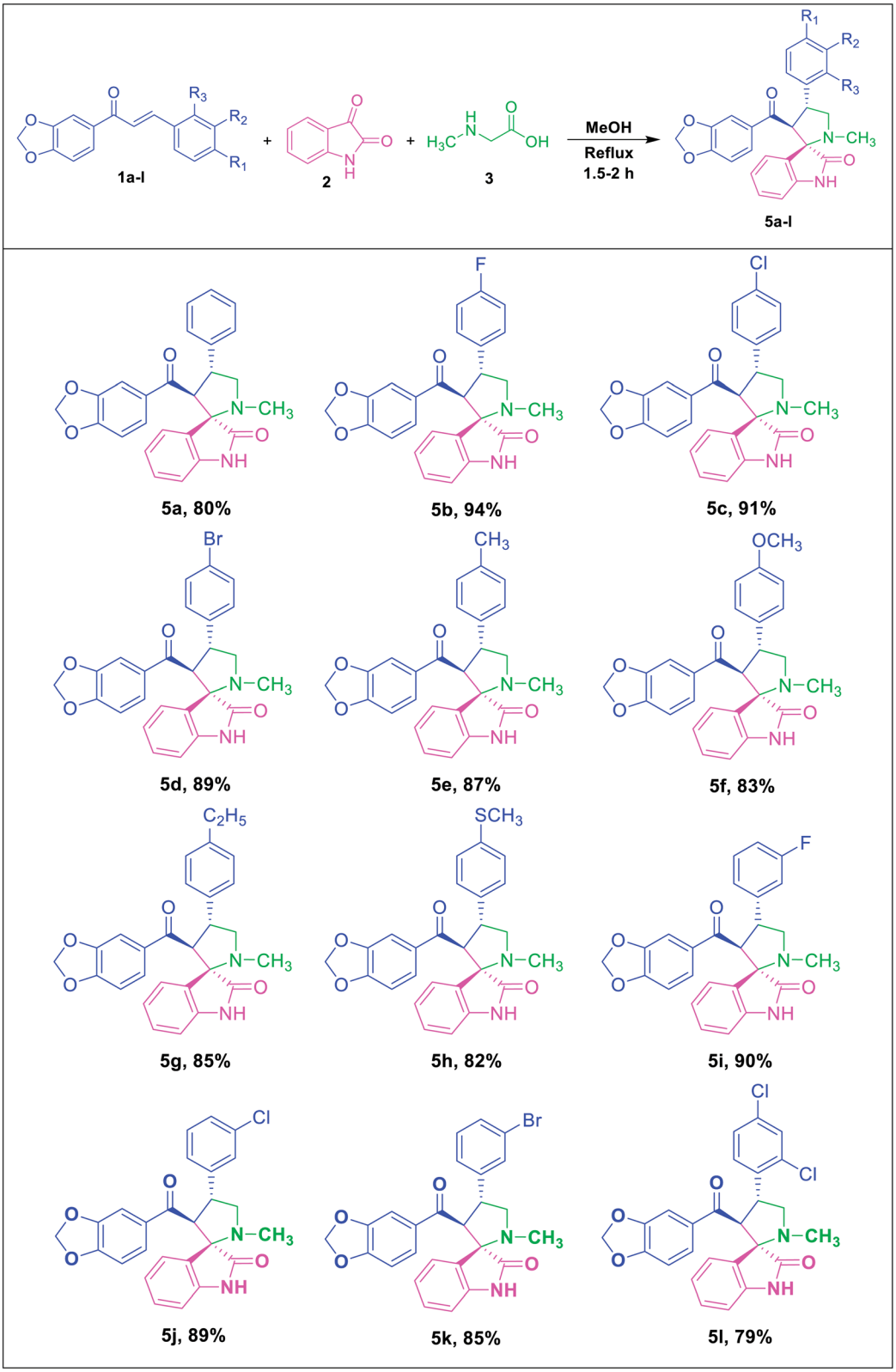

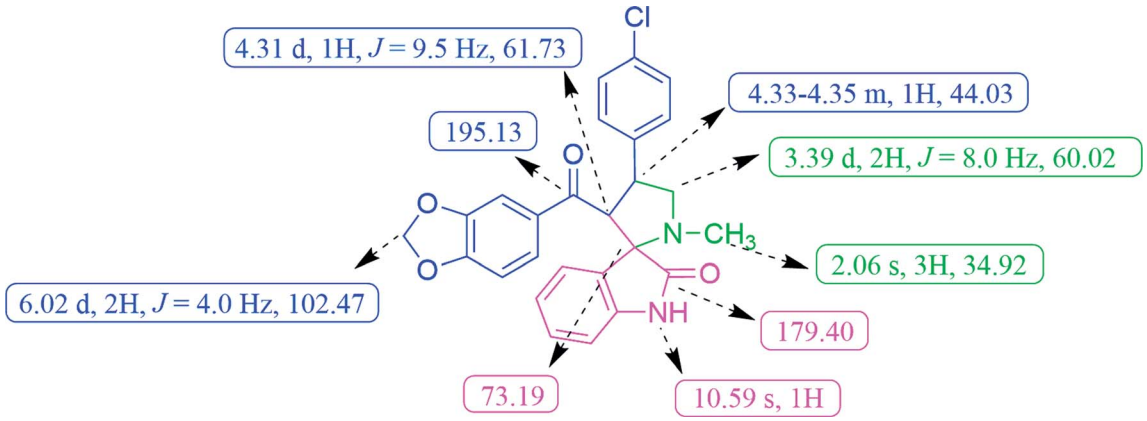

Fig. 2 Selected ^{1}H and ^{13}C NMR chemical shifts of spirooxindole pyrrolidine **5c**.

proton (H-4) of the pyrrolidine ring resonated as a multiplet at δ 4.33–4.35 (Fig. 2). The methylenedioxy protons of benzodioxole appeared at δ 6.02 as a doublet. A broad singlet at δ 10.59 was due to the oxindole –NH proton and the rest of the aromatic protons resonated between the region of δ 6.55–7.43. The ^{13}C NMR spectrum of **5c** showed the presence of 26 carbons including the carbon peaks at δ 195.13 and 179.40 for benzodioxole and oxindole ring carbonyls (Fig. 2). The methylenedioxy carbon appeared at δ 102.47, spiro carbon (C-2) at δ 73.19 and pyrrolidine N–CH_3 carbon at *d* 34.92, respectively. The peaks found at δ 44.03 and 60.02 corresponds to pyrrolidine ring methine (C-4) and methylene (C-5) carbons respectively. Additionally, the formation of compound **5c** was evidenced by the HR-MS analysis, exhibiting a characteristic $[M + H]^+$ peak at *m*/*z* 461.1269, which exactly matches with the calculated mass of the compound. Based on the above spectral data information confirmed the structure as 3′-(benzo[*d*][1,3]dioxole-5-carbonyl)-4′-(4-chlorophenyl)-1′-methylspiro[indoline-3,2′-pyrrolidin]-2-one (**5c**).

To broaden the scope and reproducibility of the above outcomes, the cycloaddition reaction was further widened. Herein, we have proposed the reaction between dipolarophile derivatives of benzodioxole chalcones (**1a–l**) with azomethine ylide generated *in situ* from isatin (**2**) and L-proline (**4**) to obtain the corresponding spirooxindole pyrrolizidine derivatives **6a–l** in good yields with high selectivity (Table 3).

The FT-IR spectrum of the compound **6c** displayed –NH group stretching at 3120 cm^{-1} and O–CH_2–O stretching at 2968 cm^{-1}. The benzodioxole and oxindole ring carbonyls appeared at 1721 and 1652 cm^{-1}, respectively. The ^{1}H NMR spectrum exhibited two multiplets at δ 1.70–1.78 and 1.84–1.89 were due to the pyrrolidine ring H-6 and H-7 methylene protons. A multiplet at δ 2.33–2.36 and a doublet of doublet at δ 2.58 were assigned to the pyrrolizidine ring H-8 methylene protons. The methine proton (H-4) was resonated as a doublet at δ 3.86, indicating the regioselectivity of the product. A multiplet that appeared at *d* 3.89–3.91 was due to the H-5 proton of the pyrrolizidine ring. The methylenedioxy protons (O–CH_2–O) was resonated as a doublet at *d* 6.04. A broad singlet at *d* 10.30 was observed due to the oxindole –NH proton and the rest of the aromatic protons resonated between the region of δ 6.59–7.48. The ^{13}C NMR spectrum showed the presence of 28 carbons, including the benzodioxole and oxindole ring carbonyl carbons at δ 194.76 and 179.86, methylenedioxy carbon at δ 102.45, and spiro carbon (C-2) at *d* 73.00, respectively. The pyrrolizidine ring of two methines (C-4 & C-5) and three methylene carbons (C-6, C-7 & C-8) were observed at δ 48.00, 71.69, 29.81, 27.11 and 52.21, respectively (Fig. 3). Moreover, the structure of 6c was further confirmed by HR-MS analysis, displaying a characteristic $[M + H]^+$ peak at *m*/*z* 487.1431.

Similarly, the formation of all other spirooxindole pyrrolizidine derivatives was confirmed by FT-IR, ^{1}H and ^{13}C NMR and HR-MS spectral data. Finally, the regio- and stereochemical outcomes of the achieved product **6i** was determined unambiguously by single crystal X-ray diffraction studies (Fig. 4).

It is expected that the nucleophilic attack of sarcosine (**3**) into the active carbonyl of isatin (**2**) involves the conversion of the carbonyl group to alcohol. The resulting OH will further attack the carboxylic group in sarcosine to obtain lactone functionality (**I**). Thus, the reactive azomethine ylide (**II**) was generated by *in situ* decarboxylative condensation reaction. Subsequently, the azomethine ylide undergoes a 1,3-dipolar cycloaddition reaction with dipolarophile (**1a**) to afford the spirooxindole pyrrolidine derivative (**5a**) in a diastereoselective and regioselective manner (Scheme 1). However, it is accepted that the cycloaddition of azomethine ylide proceeds preferentially *via* an S-shaped ylide than a W-shaped ylide because of the higher resonance energy and stability of the S-shaped ylide.[34]

The formation of regioisomer **5** could be described given the secondary orbital interaction (SOI) between the orbital of the carbonyl group of dipolarophiles with respect to azomethine ylide. The reaction between the dipolarophile and azomethine ylide is more favourable for regioisomer **5** *via* path A due to the secondary orbital interaction[35,36] while the regioisomer **5′** is not

Table 3 Substrate scope for the stereo- and regioselective synthesis of spirooxindole pyrrolizidine derivatives[a,b]

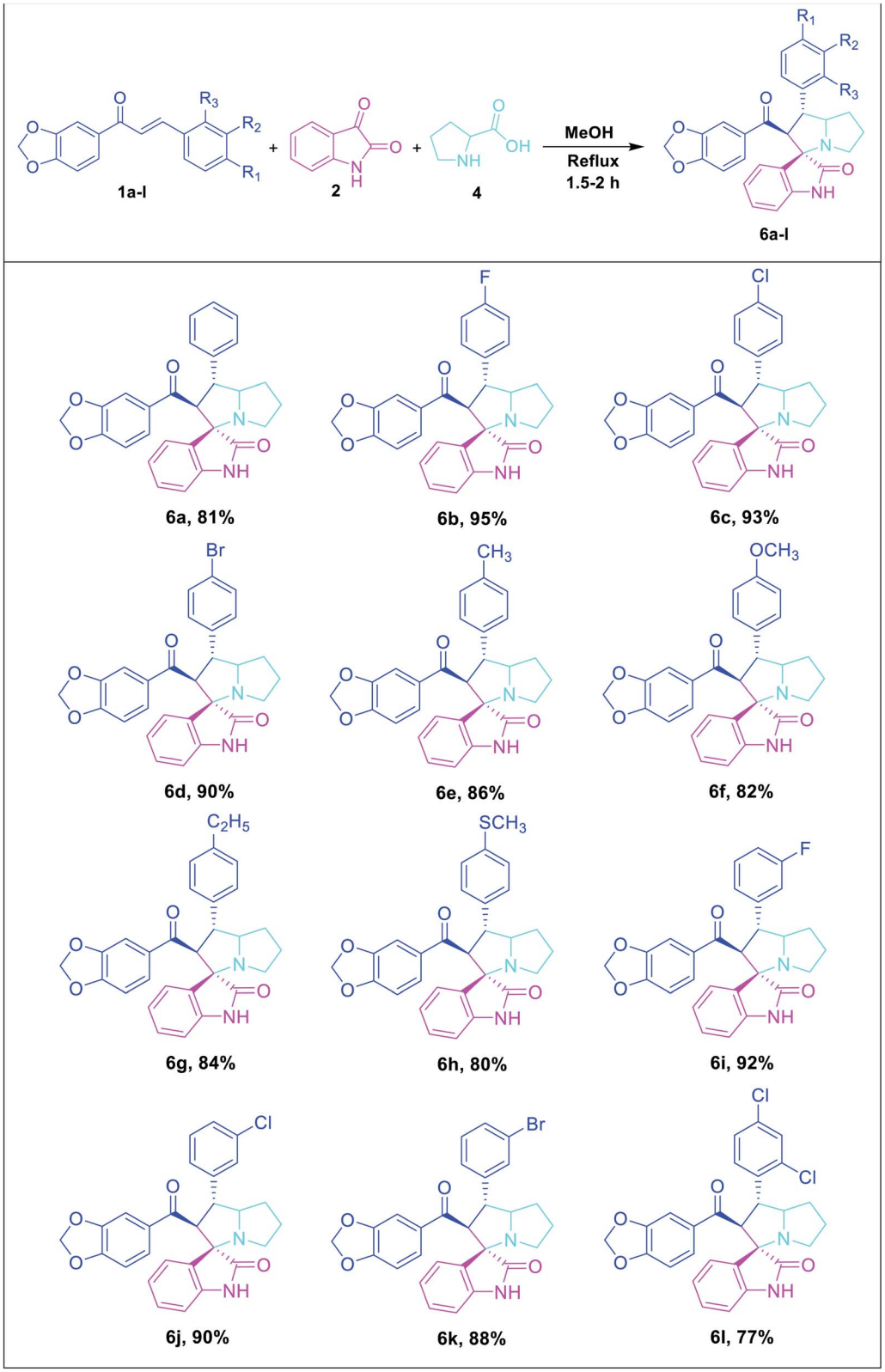

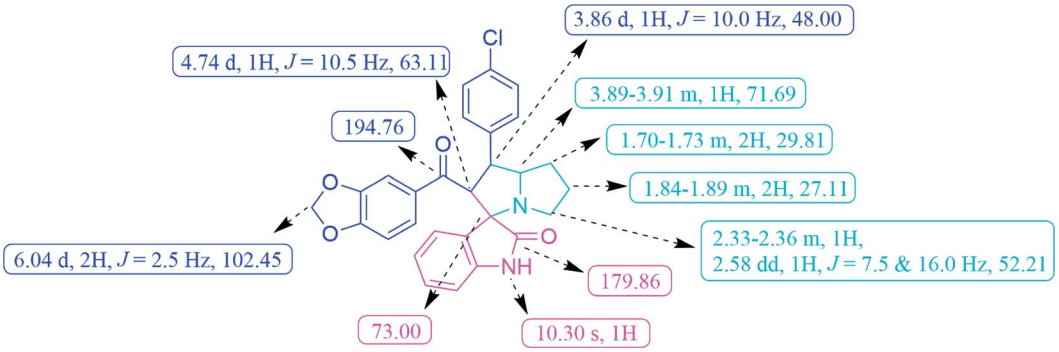

Fig. 3 Selected ^{1}H and ^{13}C NMR chemical shifts of spirooxindole pyrrolizidine **6c**.

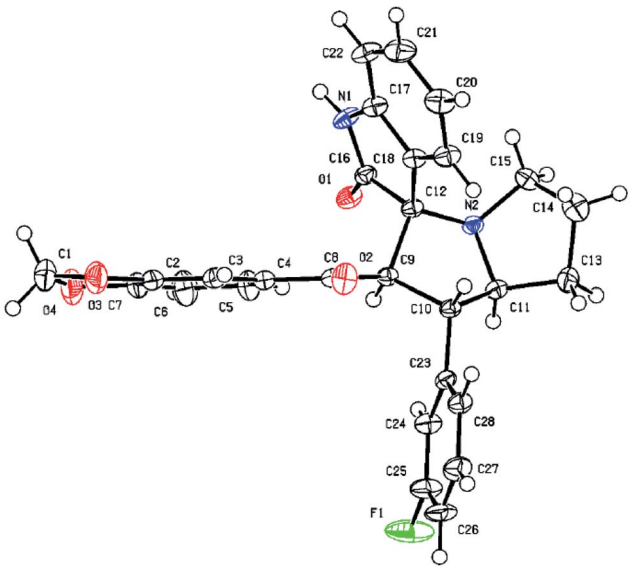

Fig. 4 ORTEP diagram of compound **6i**.

possible *via* path B (Scheme 1). Consequently, the orientation of the C_2 stereocentre is always pre-established, hence confirming the stereochemistry of the spirooxindole pyrrolidine **5**. Overall, the reaction is demonstrated to be highly regio- and stereoselective, leading to the construction of only one stereoisomer.

Single crystal X-ray diffraction studies

Single crystal X-ray diffraction analysis confirmed the structure of compound **6i** and molecular structure is shown in Fig. 4.

Collected crystal data and the refinement parameters are tabulated (See ESI†). Compound **6i** crystallized in a triclinic crystal system and space group *P*-1. Two molecular units are present in a unit cell and selected bond lengths and bond angles are shown in the ESI.† The bond lengths of C(10)–C(11); 1.535(2) Å, C(12)–C(9); 1.556 Å and N(2)–C(12); 1.472 Å were confirmed the formation of new spirooxindole pyrrolizidine derivative. Two spiro-moieties are combined with C12 asymmetric centre. From the crystal packing of **6i** molecules have a strong intermolecular hydrogen bond between C16–N1H1⋯O1.

In vitro biological studies

Inhibitory effects on yeast α-glucosidase, α-amylase and AGE formation. *In-vitro* α-glucosidase inhibitory experiments showed that **6i** had a higher inhibitory capacity than the other **5** (**5b**, **5c**, **5d**, **5e**, **5g**, **5j**, **5k**, **5l**) and **6** (**6a**, **6c**, **6g**, **6i**, **6j**, **6k**) series. The IC_{50} value for **6i** was reported to be 10.0 g mL^{-1}, while acarbose (positive control) had an IC_{50} value of 10.15 g mL^{-1} when analyzed under identical circumstances. In terms of IC_{50} values, **6i** clearly inhibited yeast α-glucosidase and was notably similar ($p < 0.05$) to acarbose while being significantly higher than other produced compounds (Table 4).

Similar tests were carried out to see if series **5** (**5b**, **5c**, **5d**, **5e**, **5g**, **5j**, **5k**, **5l**) and series **6** (**6a**, **6c**, **6g**, **6i**, **6j**, **6k**) inhibited α-amylase, another important carbohydrate hydrolyzing enzyme. In comparison to the other compounds tested, **6i** (IC_{50} : 32.40 g mL^{-1}) had the strongest inhibitory action against α-amylase, whereas **5b** (IC_{50} : 70.50 g mL^{-1}) had the lowest inhibitory impact, as indicated in Table 4. All of the substances examined had IC_{50} values that were significantly higher ($p < 0.05$) than the medicinal medication acarbose (IC_{50} : 30.05 g mL^{-1}).

The inhibitory effects of various doses of test compounds and aminoguanidine (25, 50, and 100 g mL^{-1}) on AGE after 3 weeks of incubation are shown in Fig. 5. Albumin glycation was reduced in a dose-dependent manner after incubation with series **5** (**5b**, **5c**, **5d**, **5e**, **5g**, **5j**, **5k**, **5l**) and series **6** (**6a**, **6c**, **6g**, **6i**, **6j**, **6k**). By the end of the trial, it was obvious that **6i** had greater inhibitory activity against AGE than the other test compounds tested at varying doses. The fluorescence experiments on AGE, as shown in Fig. 5A and B concluded that compounds inhibit in the range of 50–75% at a concentration of 100 g mL^{-1}. On a 21 day incubation period, **6i** showed stronger inhibition than a well-known inhibitor, aminoguanidine, at various doses.

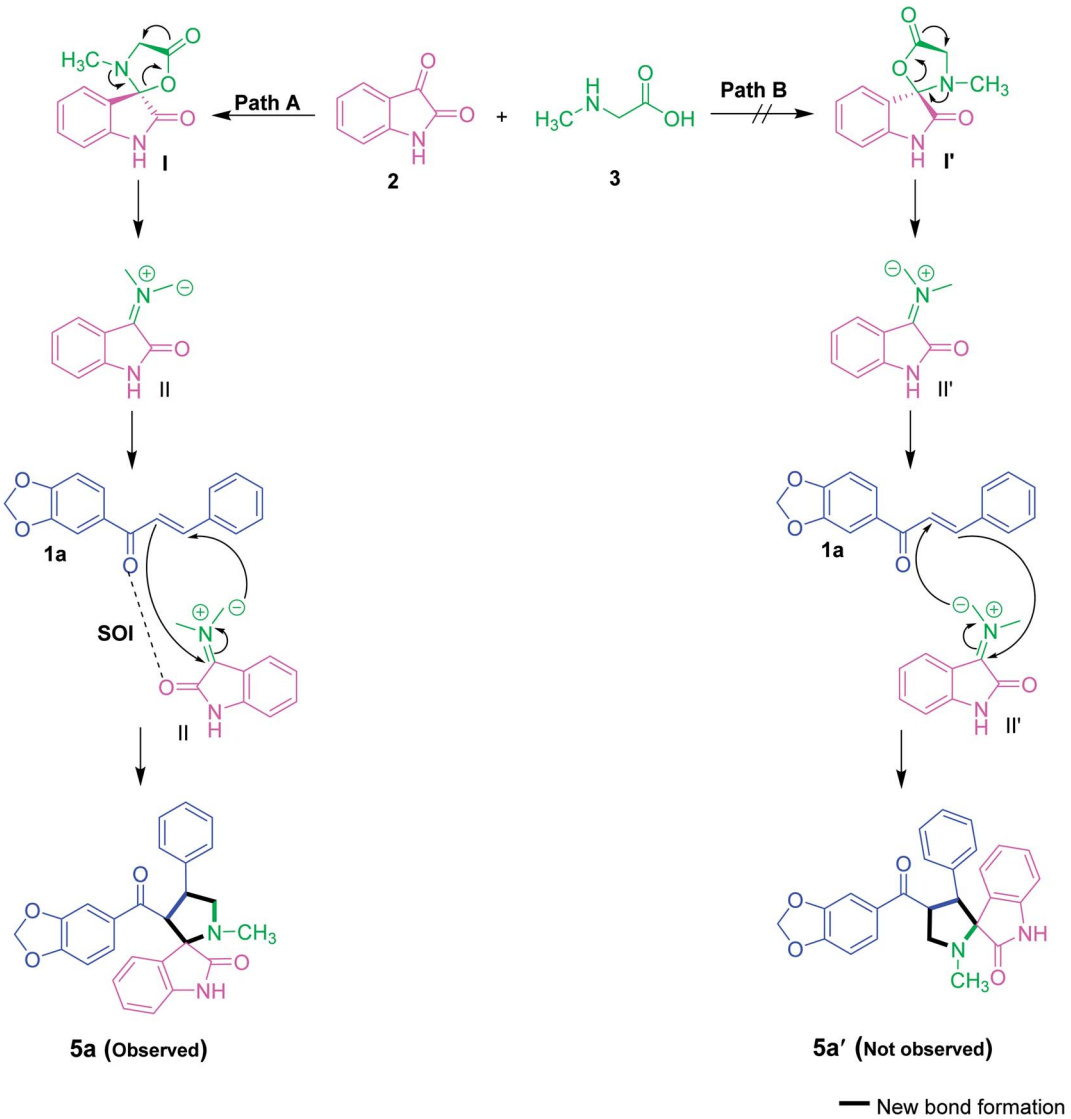

Scheme 1 Proposed reaction mechanism for the synthesis of **5**.

In silico biological studies

Molecular docking simulation. The virtual screening of series 5 and 6 compounds, predicted **6i** as a potent inhibitor of α-glucosidase, α-amylase, and human serum albumin proteins, with the binding affinity of −10.1, −8.9, −10.0 kcal mol^{-1}, respectively. The results obtained for the respective control drugs were not significant due to the comparatively positive binding affinities and extent of binding interaction with protein amino-acid residues. Compound **6i** also formed higher number of non-bonded and hydrogen bonds with the target proteins, which could result in the significant binding affinity in comparison with control drugs. Table 5 details the results of virtual screening of experimental compounds docked against the target proteins. Details of binding interactions of **6i** and respective ligands with the target proteins have been given in Table 6 (for α-glucosidase), Table 7 (for α-amylase), and Table 8 (for human serum albumin). Likewise, visualization of binding interaction has been depicted Fig. 6 (for α-glucosidase), Fig. 7 (for α-amylase), and Fig. 8 (for human serum albumin).

Molecular dynamics simulation

Molecular dynamics simulation is performed to evaluate the conformational stabilities of protein-ligand complexes. For all the protein-ligand complexes, the RMSD, RMSF, Rg, and SASA graphs were plotted. The graphical representation of molecular dynamics simulation for α-glucosidase, α-amylase, and human

Table 4 Inhibitory activities of spirooxindole pyrrolidinyl derivatives against α-amylase and α-glucosidase enzymes

	Enzymes IC_{50}[a]a, [b]b (μg mL^{-1})	
Test Compounds	α-amylase	α-glucosidase
5b	70.50 ± 0.50 [f]	46.15 ± 1.30 [g]
5c	46.00 ± 0.44 [c]	17.66 ± 1.90 [b]
5d	35.78 ± 2.06 [b]	12.05 ± 0.13 [b]
5e	36.80 ± 1.04 [b]	14.75 ± 0.02 [c]
5g	45.50 ± 2.31 [c]	24.05 ± 1.86 [e]
5j	62.04 ± 0.81 [e]	30.00 ± 1.77 [f]
5k	50.75 ± 0.07 [d]	25.03 ± 0.63 [e]
5l	44.80 ± 0.32 [c]	18.20 ± 0.86 [d]
6a	63.00 ± 0.36 [e]	26.00 ± 1.02 [e]
6c	44.25 ± 0.05 [c]	18.03 ± 1.00 [d]
6g	35.00 ± 0.35 [b]	14.00 ± 0.50 [c]
6i	**32.40 ± 0.86** [a]	**10.00 ± 0.16** [a]
6j	50.50 ± 1.00 [d]	15.00 ± 0.00 [c]
6k	62.05 ± 1.11 [e]	29.55 ± 0.08 [f]
Standard [c]	30.05 ± 0.05 [a]	10.15 ± 0.06 [a]

[a] All the values are expressed as mean ± SE. Means in the same column with diverse superscripts are significantly different ($p \leq 0.05$) as per separated by Duncan multiple range test. [b] The IC_{50} value is defined as the inhibitor concentration to inhibit 50% of enzyme activity under assay conditions. [c] Standard: Acarbose (positive control).

serum albumin has been given in Figures 9–11, respectively. The RMSD plot of the protein-ligand complex displays the stability of the ligand and protein over the course of a 100 ns simulation. All the RMSD trajectories found in this simulation were found to be stable after 20 ns, free from initial fluctuations. In the case of α-glucosidase, RMSD of both protein-**6i** and protein-acarbose complexes were predicted to be within the range of 0.30–0.40 nm. However, protein backbone atoms were also found with the same pattern as both complexes. In the case of α-amylase, the protein-**6i** complex was found to be in the range of 0.4–0.5 nm. Yet both protein backbone atoms and protein-acarbose complex were in the range of 0.3–0.4 nm. Further, RMSD of protein-**6i** and protein backbone atoms in case of human serum albumin were found to be in the range of 0.5–0.6 nm. Yet, the protein-aminoguanidine complex predicted showed the fluctuation in the RMSD of 0.75 nm at 62 ns.

The average deviation of a particle (*e.g.*, a protein residue) from a reference location over time is calculated using RMSF. As a result, RMSF focuses on the regions of the protein structure that deviate the most/least from the mean. In the case of all the three protein backbone atoms, fluctuations were observed only during N- and C-terminals as well as loop regions. However,

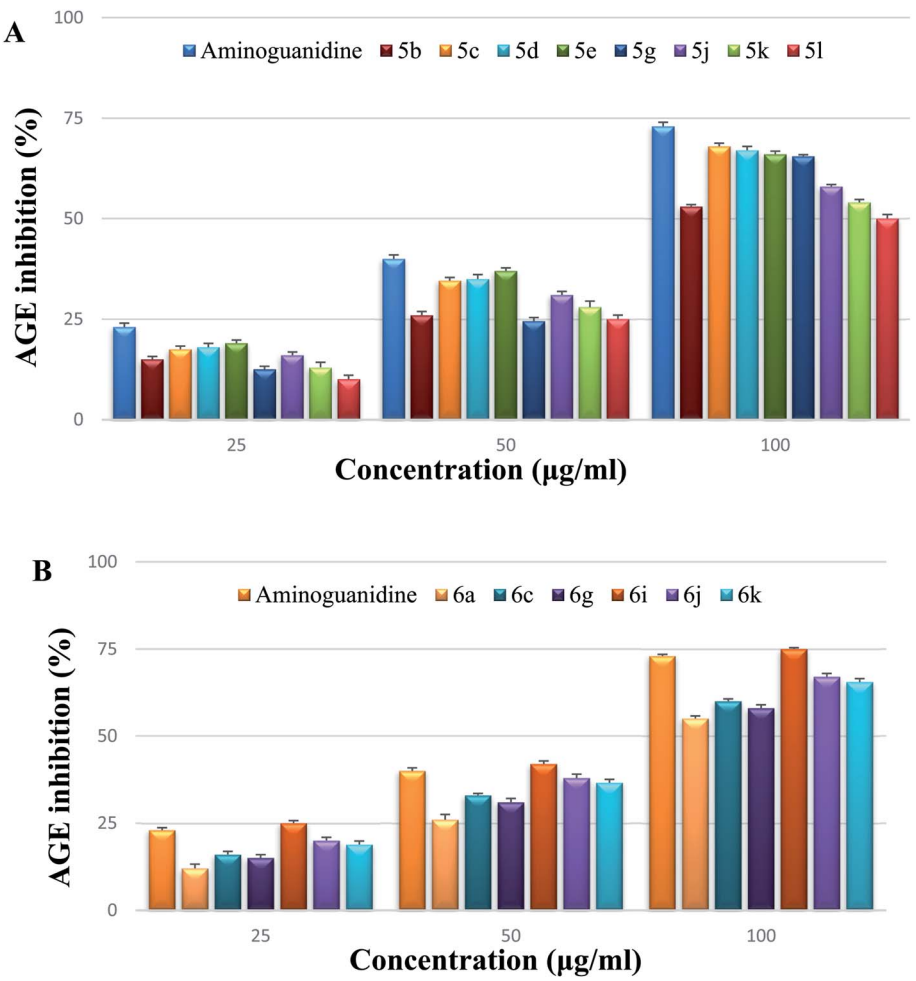

Fig. 5 (A) Inhibitory effects of series **5** spirooxindole pyrrolidine derivatives on AGE formation at diverse concentrations. (B) Inhibitory effects of series **6** spirooxindole pyrrolizidine derivatives on AGE formation at diverse concentrations.

Table 5 Binding affinity, non-bonding and hydrogen bonding interactions of compounds with their respective target proteins

Sl. No.	Name of the compound	Binding affinity (kcal mol^{-1})			Total no. of non-bonded interactions			Total no. of hydrogen bonds		
		α-glucosidase	α-amylase	Human serum albumin	α-glucosidase	α-amylase	Human serum albumin	α-glucosidase	α-amylase	Human serum albumin
1	**5b**	−10.2	−8.4	−9.1	12	8	9	4	3	2
2	**5c**	−9.5	−8.1	−8.8	16	9	5	3	2	1
3	**5d**	−11.1	−8.6	−9.2	14	8	10	3	3	2
4	**5e**	−10.2	−8.4	−9.7	21	10	12	9	4	4
5	**5g**	−9.6	−8.1	−8.9	11	9	12	1	3	—
6	**5j**	−9.5	−7.9	−8.8	9	11	12	1	2	2
7	**5k**	−9.7	−8.0	−9.1	15	7	14	4	2	—
8	**5l**	−9.9	−8.5	−8.6	16	14	12	4	7	3
9	**6a**	−10.0	−8.3	−9.5	15	9	16	2	2	1
10	**6c**	−10.1	−8.2	−9.3	15	11	16	4	1	1
11	**6g**	−10.1	−8.9	−10.0	15	13	19	5	4	8
12	**6i**	**−10.1**	**−8.5**	**−9.9**	**13**	**11**	**13**	**3**	**2**	**1**
13	**6j**	−10.5	−8.2	−9.7	17	12	14	3	3	3
14	**6k**	−10.0	−8.2	−8.8	15	8	6	2	2	1
15	Acarbose	−8.6	−6.0	—	10	6	—	9	6	—
16	Aminoguanidine	—	—	−4.1	—	—	6	—	—	4

Table 6 Binding interaction of ligand with **6i** and acarbose with α–glucosidase along with their respective distance

Sl. No.	Name of the compound	Binding affinity (kcal mol^{-1})	Hydrogen bonds	Electrostatic bonds	Hydrophobic bonds			
					Pi-sigma	Pi- Pi bond	Alkyl	Pi-alkyl
1	**6i**	−10.1	HIS A: 279 (2.86), HIS A: 279 (2.86), ARG A: 312 (2.93), ARG A: 312 (2.45), PHE A: 157 (3.47)	HIS A: 279 (4.60), GLU a:304 (4.10)	—	PHE A: 157 (4.73), UNL1 (5.37)	ARG A: 312 (4.31)	LEU A: 218 (5.42), ALA A: 278 (3.07), LEU A: 218 (4.06), ALA A: 278 (3.04), ARG A: 312 (4.81)
2	Acarbose	−8.6	ASN A: 241 (2.31), HIS A: 279 (2.77), ARG A: 439 (2.48), PRO A: 309 (2.33), HIS A: 279 (2.82), PRO A: 309 (2.33), HIS A: 239 (2.25), HIS A: 279 (2.98), ARG A: 439 (2.44)	—	HIS A: 279 (3.58)	—	—	—

Table 7 Binding interaction of ligand with **6i** and acarbose with α-amylase along with their respective distance

Sl. No.	Name of the compound	Binding affinity (kcal mol^{-1})	Hydrogen bonds	Electrostatic bonds	Halogen	Hydrophobic bonds			
						Pi-sigma	Pi–Pi bond	Alkyl	Pi-alkyl
1	**6i**	−8.9	LYS A: 457 (2.91), LYS A: 457 (2.82), SER A: 494 (2.71), SER A: 494 (2.32)	LYS A: 457 (3.73), LYS A: 457 (3.43)	GLU A: 493 (3.14)	—	TRP A: 396 (3.92), TRP A: 396 (5.21)	—	TRP A: 396 (4.91), TRP A: 396 (4.32), LYS A: 457 (4.54), LYS A: 457 (5.03)
2	Acarbose	−6.0	ARG A: 343 (1.88), ARG A: 343 (6.15), ARG A: 392 (2.14), CYS A: 378 (2.46), GLU A: 390 (2.96), ASP A: 456 (2.56)	—	—	—	—	—	—

Table 8 Binding interaction of ligand with 6i and aminoguanidine with Human serum albumin along with their respective distance

Sl. No.	Name of the compound	Binding affinity (kcal mol^{-1})	Hydrogen bonds	Electrostatic bonds	Hydrophobic bonds				
					Amide-Pi Stacked	Pi-sigma	Pi–Pi bond	Alkyl	Pi-alkyl
1	**6i**	−10.0	LYS A: 195 (2.34), ARG A: 218 (2.43), ARG A: 218 (3.09), ARG A: 218 (2.46)	—	PRO A: 447 (4.11)	—	HIS A: 440 (4.51), UNL1 (5.14)	LYS A: 195 (4.43), VAL A: 455 (4.51)	TYR A: 452 (5.00), LYS A: 436 (5.01), CYS A: 448 (5.42), PRO A: 447 (5.16), CYS A: 448 (4.04), LYS A: 444 (4.80), PRO A: 447 (5.34), CYS A: 448 (3.99), LYS A: 195 (5.19)
2	Aminoguanidine	−4.1	ASP A: 108 (1.97), LYS A: 106 (2.48), LEU A: 103 (2.66), LYS A: 106 (1.91)	GLU A: 465 (2.39), ASP A: 108 (2.89)	—	—	—	—	—

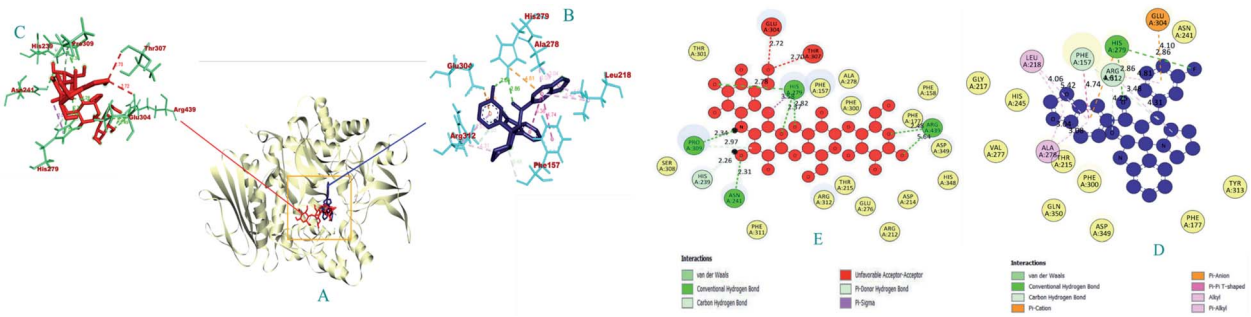

Fig. 6 The 3D and 2D interaction view of compound **6i** with the binding sites of α-glucosidase.

protein-**6i** complexes were found with minimal fluctuations in all the 3 simulations run. Whereas, protein-acarbose and protein-aminoguanidine complexes were found with more fluctuations.

The radius of gyration (Rg) of proteins and protein-ligand complexes was plotted because it reflects the structural compactness of the molecules by considering the variable masses determined to root mean square distances with respect to the central axis of rotation. In this study, Rg of α-glucosidase protein backbone atoms was found to be ranging between 3.0–3.5 nm. Whereas, Rg of both protein-**6i** and the protein–acarbose complex was found to be in the same pattern, between 2.0-2.5 nm. In the case of α-amylase, Rg of protein backbone was found to be ranging between 2.2-2.3 nm, protein-**6i** between

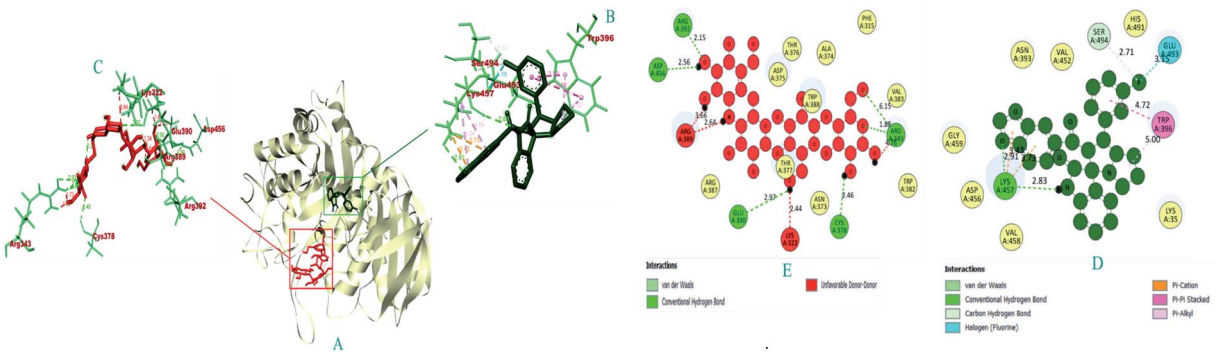

Fig. 7 The 3D and 2D interaction view of compound **6i** with the binding sites of α-amylase.

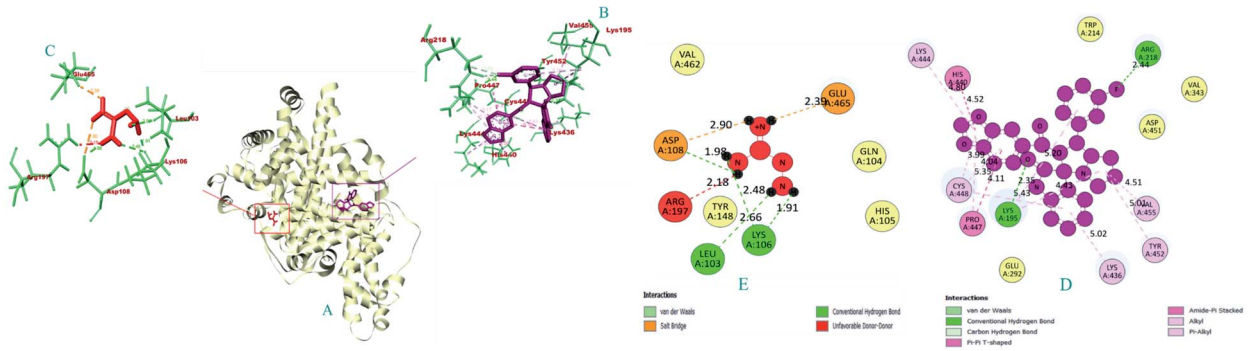

Fig. 8 The 3D and 2D interaction view of compound **6i** with the binding site of Human serum albumin.

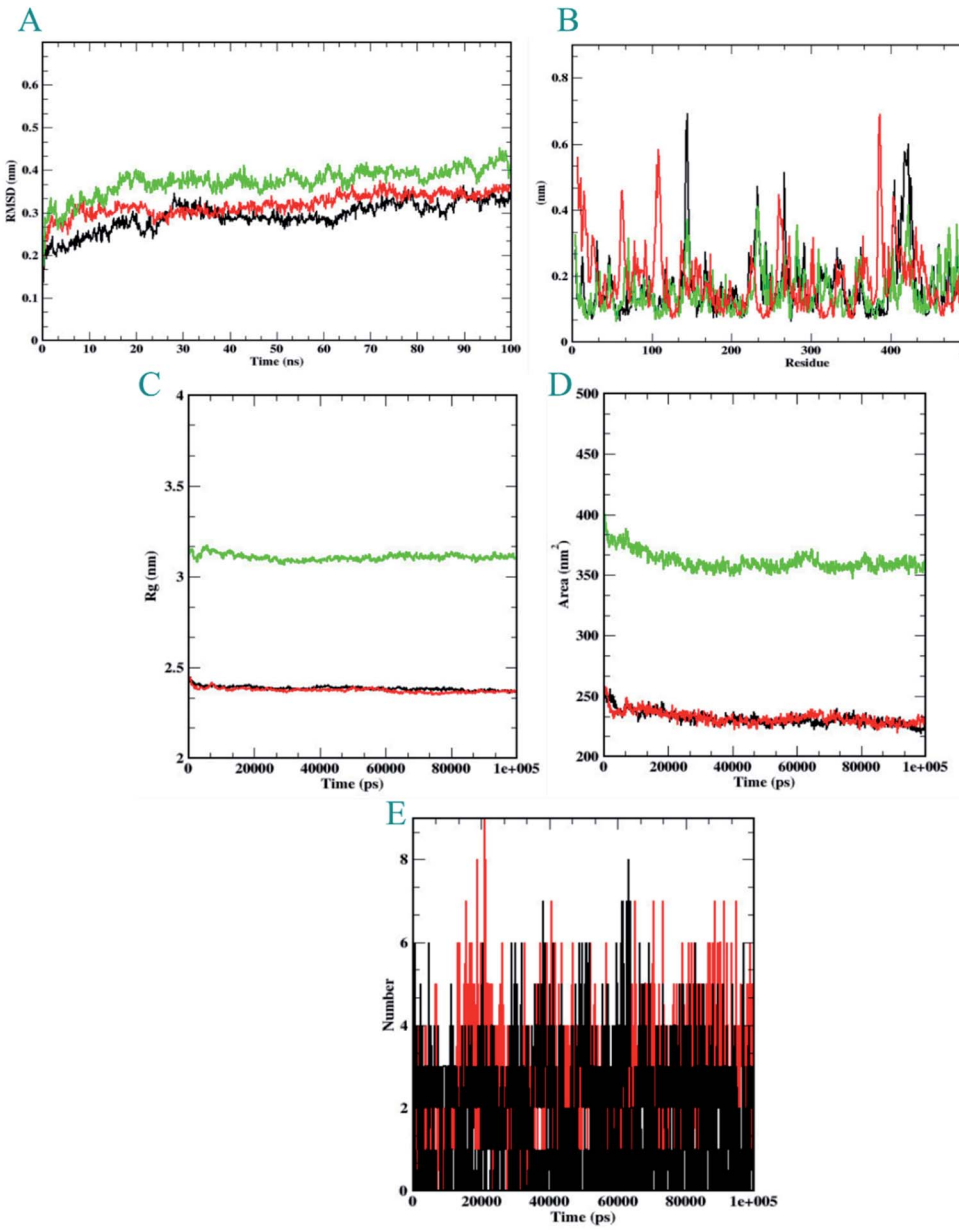

Fig. 9 Analysis of RMSD, RMSF, Rg, SASA, and number of hydrogen bonds of **6i** (black) and acarbose (red) with α–glucosidase (green) at 100 ns. (A) Time evolution of backbone RMSD of the complex structure. (B) RMSF of protein and ligand. (C) The radius of gyration (Rg) (D) SASA (E) Hydrogen bonds occurring over the time of simulation between protein and ligand.

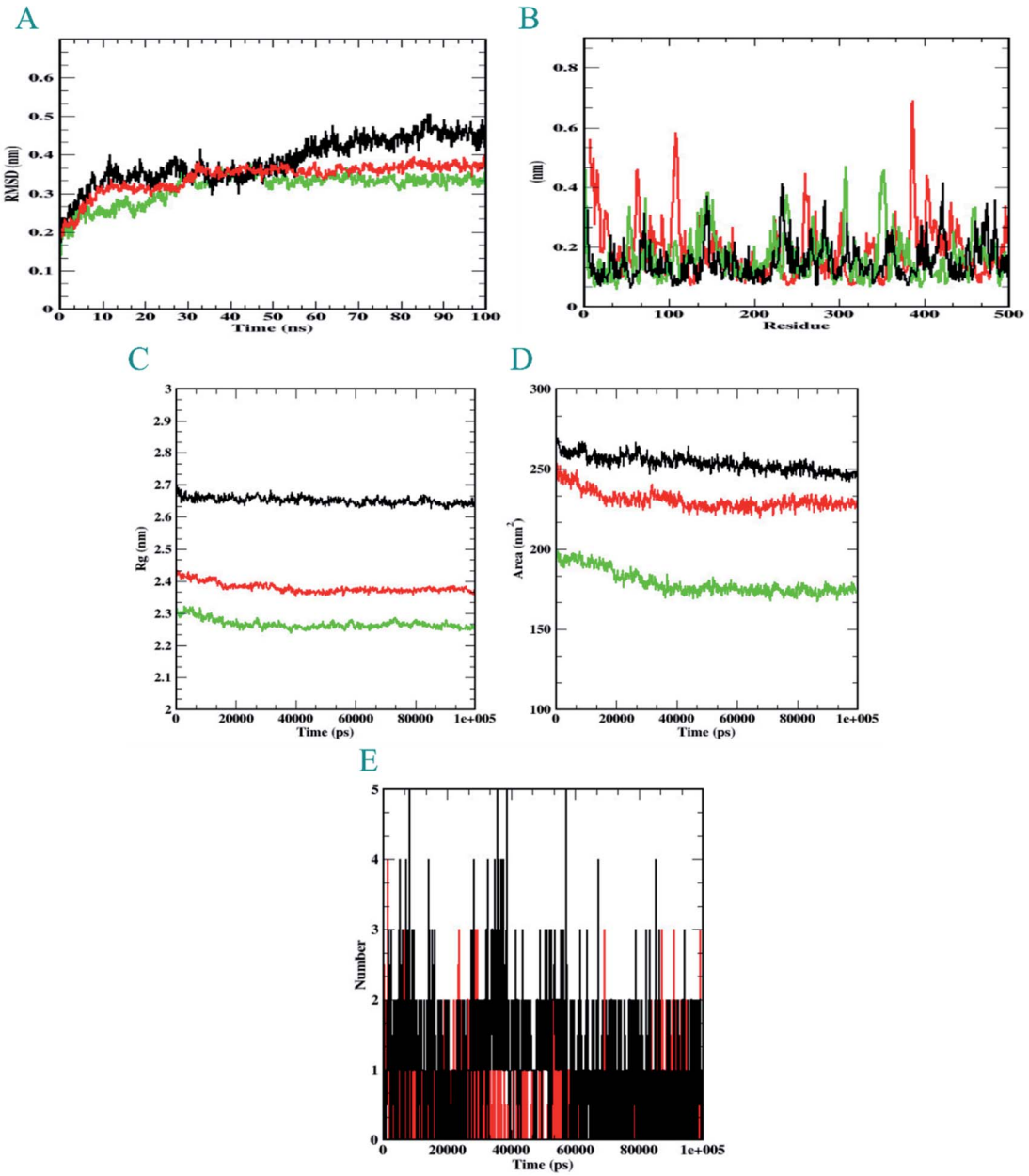

Fig. 10 Analysis of RMSD, RMSF, Rg, SASA, and number of hydrogen bonds of **6i** (black) and acarbose (red) with α-amylase (green) at 100 ns. (A) Time evolution of backbone RMSD of the complex structure. (B) RMSF of protein and ligand. (C) The radius of gyration (Rg) (D) SASA (E) Hydrogen bonds occurring over the time of simulation between protein and ligand.

2.6–2.7, and protein-acarbose between 2.3–2.4 nm. All three trajectories were predicted with different Rg values. However, in the case of human serum albumin, protein-**6i** complex the average Rg was found to be between 2.6–2.66 and protein-aminoguanidine had the same pattern of Rg with 2.68–2.7 nm. Whereas, protein backbone atoms were predicted with 2.6 nm of Rg value.

Furthermore, the area around the hydrophobic core created between protein-ligand complexes was shown in SASA plots for all of the protein-ligand complexes. In the case of α-glucosidase, the protein backbone atoms were found with the SASA value of ~350 nm^2 and both ligand complexes were predicted with 200–250 nm^2. In the case of α-amylase, all the three SASA directories had different values. Protein backbone atoms were predicted with 155–200 nm^2, protein-**6i** complex with ~250 nm^2, and protein-acarbose with 200–250 nm^2 SASA value. Conversely, all three trajectories had the same pattern of SASA value in case of

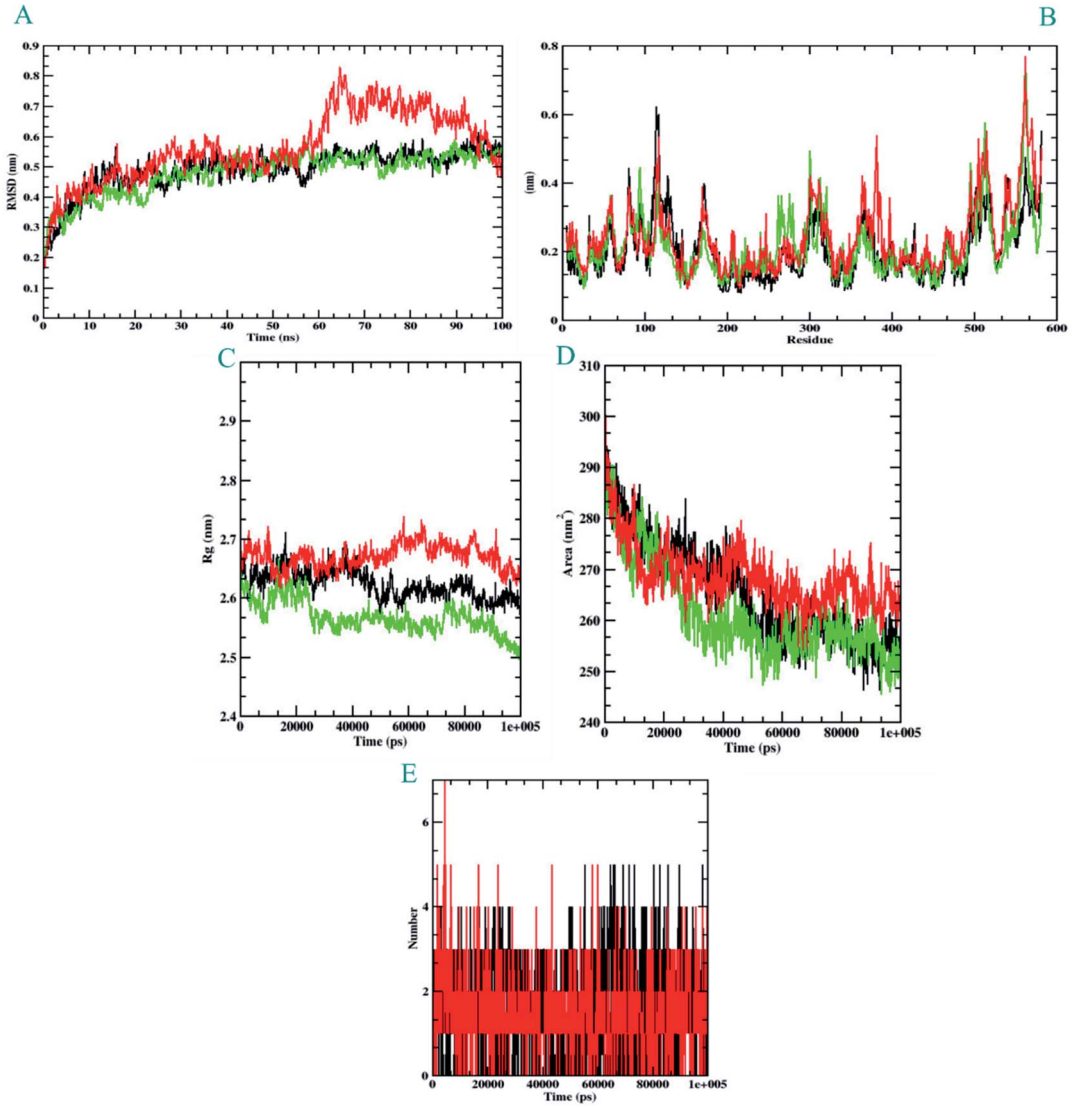

Fig. 11 Analysis of RMSD, RMSF, Rg, SASA, and the number of hydrogen bonds of **6i** (black) and Aminoguanidine (red) with Human serum albumin (green) at 100 ns. (A) Time evolution of backbone RMSD of the complex structure. (B) RMSF of protein and ligand. (C) The radius of gyration (Rg) (D) SASA (E) hydrogen bonds occurring over the time of simulation between protein and ligand.

human serum albumin. All the trajectories were predicted to have the SASA value between 250–290 nm^2.

Furthermore, it is essential to calculate the number of H-bonds formed during the simulation, as few bonds were simultaneously broken and rebuilt. During the simulation with α-glucosidase, acarbose had formed 9, while **6i** formed 8 hydrogen bonds. In the case of α-amylase, **6i** edged over acarbose to form 5 bonds, whereas, acarbose had 4 hydrogen bonds. Whereas, in the case of human serum albumin, where aminoguanidine had formed 7 hydrogen bonds, however, **6i** formed 5 of them. Therefore, by considering all the MD trajectories, it can be deduced that compound **6i** had stability and extensive interaction in the case of all three proteins.

Binding free energy calculations

Evaluation of binding free energies is essential, as the concept dwells with the stability and extent of binding interaction of ligands with the protein. In all the protein-ligand complexes formed, acarbose, aminoguanidine and **6i** used van der Waals's energy to form the complexes. This was followed by binding energy. Polar solvation energy was found to be not involved with the protein-ligand complexes, as most of the values were positive. Moreover, the binding free energies of the protein-**6i** complex were comparatively more negative (stable complex) than both the controls. In addition, the binding free energies shown by the protein-control drug complexes were deviating from the real values. This shows that the binding of **6i** with all

Table 9 Binding free energy calculations of 6i with their respective proteins

	6i- α-glucosidase complex		Acarbose- α-glucosidase complex		6i- α-amylase complex		Acarbose- α-glucosidase complex		6i- Human serum albumin complex		Aminoguanidine-Human serum albumin complex	
	Values (kJ mol^{-1})	Standard deviation (kJ mol^{-1})	Values (kJ mol^{-1})	Standard deviation (kJ mol^{-1})	Values (kJ mol^{-1})	Standard deviation (kJ mol^{-1})	Values (kJ mol^{-1})	Standard deviation (kJ mol^{-1})	Values (kJ mol^{-1})	Standard deviation (kJ mol^{-1})	Values (kJ mol^{-1})	Standard deviation (kJ mol^{-1})
van der Waal energy	−316.391	±15.473	−218.605	±145.706	−169.669	±101.479	−150.112	±115.233	−231.156	±12.251	−37.584	±17.357
Electrostatic energy	−21.871	±5.801	−4.761	±6.221	−6.992	±11.374	−10.911	±6.801	−23.992	±10.977	−19.990	±12.655
Polar solvation energy	107.897	±13.989	103.307	±55.952	79.945	±50.793	60.951	±25.681	125.581	±30.228	38.908	±29.180
SASA energy	−21.576	±0.997	−17.835	±13.498	−12.899	±7.329	−15.929	±6.997	−19.988	±1.220	−5.720	±1.880
Binding energy	−251.941	±22.094	−137.894	±122.951	−109.615	±73.901	−112.119	±46.114	−149.555	±26.000	−24.385	+/20.763

the 3 target proteins is stable and stronger, in comparison with the control drugs. The details of binding free energy calculations are given in Table 9.

Conclusion

In summary, we have developed a highly efficient synthesis of spirooxindole pyrrolidine (**5a–l**) and pyrrolizidine (**6a–l**) by 1,3-dipolar cycloaddition reaction of benzodioxole chalcones (**1a–l**) with azomethine ylide generated by the reaction of isatin (**2**) and sarcosine (**3**)/L-proline (**4**) in presence of methanol to afford desired products in high yield. The stereochemistry of the products was unambiguously confirmed by FT-IR, NMR and HR-MS techniques. Additionally, the formation of a single regio- and stereoselective of the desired products were confirmed by single crystal X-ray diffraction studies of compound 6i (CCDC: 2143927). Among the synthesized mono-spirooxindole compounds, compound **6i** showed stronger inhibition against α-glucosidase and α-amylase enzymes. This can be attributed to the presence of the fluoro-group in the C-3 position, which results in the enhanced activity. Among the synthesized spiro heterocyclic motifs, compounds **6** exhibited stronger activity against α-glucosidase and α-amylase enzymes. This is probably due to the presence of oxindole and pyrrolizidine rings, which enhanced the diabetic activity. Further, comparing the IC_{50} values of standard drugs under similar conditions shown that, the IC_{50} values for the spirooxindole derivatives are significantly lower than their conventional counterparts, demonstrating excellent diabetic efficacy of the spirooxindole substrates.

Conflicts of interest

There are no conflicts to declare.

Notes and references

1 B. Ganem, *Acc. Chem. Res.*, 2009, **42**, 463–472.
2 J. D. Sunderhaus and S. F. Martin, *Chem.–Eur. J.*, 2009, **15**, 1300–1308.
3 B. Yu, D. Q. Yu and H. M. Liu, *Eur. J. Med. Chem.*, 2015, **97**, 673–698.
4 C. Marti and E. M. Careira, *Eur. J. Med. Chem.*, 2003, **12**, 2209–2219.
5 (*a*) C. Teja, S. N. Babu, A. Noor, J. A. Daniel, S. A. Devi, F. Rahman and N. Khan, *RSC Adv.*, 2020, **10**, 12262–12271; (*b*) A. Toumi, S. Boudriga, K. Hamden, M. Sobeh, M. Cheurfa, M. Askri, M. Knorr, C. Strohmann and L. Brieger, *Bioorg. Chem.*, 2021, **106**, 104507.
6 A. Thangamani, *Eur. J. Med. Chem.*, 2010, **45**, 6120–6126.
7 (*a*) K. Ding, Y. Lu, Z. Nikolovska-Coleska, G. P. Wang, S. Qiu, S. Shangary, W. Gao, D. G. Qin, J. Stuckey, K. Krajewski, P. P. Roller and S. M. Wang, *J. Am. Chem. Soc.*, 2005, **127**, 10130–10131; (*b*) K. Ding, Y. P. Lu, Z. Nikolovska-Coleska, G. P. Wang, S. Qiu, S. Shangary, W. Gao, D. G. Qin, J. Stuckey, K. Krajewski, P. P. Roller and S. M. Wang, *J. Med. Chem.*, 2006, **49**, 3432–3435.

8 B. K. S. Yeung, B. Zou, M. Rottmann, S. B. Lakshminarayana, S. H. Ang, S. Y. Leong, J. Tan, J. Wong, S. Keller-Maerki, C. Fischi, A. Goh, E. K. Schmitt, P. Krastel, E. Francotte, K. Kuhen, D. Plouffe, K. Henson, T. Wagner, E. A. Winzeler, F. Petersen, B. Reto, V. Dartois, T. T. Diagana and T. H. Keller, *J. Med. Chem.*, 2010, **53**, 5155–5164.

9 K. Lundahl, J. Schut, J. L. M. A. Schlatmann, G. B. Paerels and A. Peters, *J. Med. Chem.*, 1972, **15**, 129–132.

10 (*a*) M. M. Khafagy, A. H. F. A. El Wahas, F. A. Eid and A. M. El Agrody, *Farmaco*, 2002, **57**, 715–722; (*b*) P. R. Sebahar and R. M. Williams, *J. Am. Chem. Soc.*, 2000, **122**, 5666–5667; (*c*) A. Bertamino, C. Aquino, M. Sala, N. D. Simone, C. A. Mattia, L. Erra, S. Musella, P. Iannelli, A. Carotenuto, P. Grieco, E. Novellino, P. Campiglia and I. Gomez-Monterrey, *Bioorg. Med. Chem.*, 2010, **18**, 4328–4337.

11 (*a*) T. H. Kang, K. Matsumoto, Y. Murakami, H. Takayama, M. Kitajima, N. Aimi and H. Watanabe, *Eur. J. Pharmacol.*, 2002, **444**, 39–45; (*b*) C. V. Galliford and K. A. Scheidt, *Angew. Chem., Int. Ed.*, 2007, **46**, 8748–8758.

12 J. Rodriguez and D. Bonne, *Stereoselective Multiple Bond-Forming Transformations in Organic Synthesis*, John Wiley & Sons, Inc., New Jersey, 1st edn, 2015.

13 (*a*) A. R. Suresh Babu, R. Raghunathan, G. Gayatri and G. N. Sastry, *J. Heterocycl. Chem.*, 2006, **43**, 1467–1472; (*b*) A. A. Watson, G. W. J. Fleet, N. Asano, R. J. Molyneux and R. J. Nash, *Phytochemistry*, 2001, **56**, 265–295; (*c*) D. O'Hagan, *Nat. Prod. Rep.*, 1997, **14**, 637–651; (*d*) S. Horri, H. Fukase, T. Matsuo, Y. Kameda, N. Asano and K. Matsui, *J. Med. Chem.*, 1986, **29**, 1038–1046; (*e*) M. A. Spearman, J. C. Jamieson and J. A. Wright, *Exp. Cell Res.*, 1987, **168**, 116–126; (*f*) A. Karpas, G. W. J. Fleet, R. A. Dwek, S. Petursson, S. K. Mamgoong, N. G. Ramsden, G. S. Jacob and T. W. Rademacher, *Proc. Natl. Acad. Sci. U. S. A.*, 1988, **85**, 9229–9233; (*g*) J. R. Liddell, *Nat. Prod. Rep.*, 1998, **15**, 363–370; (*h*) J. P. Michael, *Nat. Prod. Rep.*, 1997, **14**, 619–636.

14 (*a*) T. Hashimoto and K. Maruoka, *Chem. Rev.*, 2015, **115**, 5366–5412; (*b*) Y. Gu, *Green Chem.*, 2012, **14**, 2091–2128; (*c*) R. C. Cioc, E. Ruijter and R. V. A. Orru, *Green Chem.*, 2014, **16**, 2958–2975; (*d*) A. Nagaraju, B. J. Ramulu, G. Shukla, A. Srivastava, G. K. Verma, K. Raghuvanshi and M. S. Singh, *Green Chem.*, 2015, **17**, 950–958; (*e*) M. Li, A. Taheri, M. Liu, S. Sun and Y. Gu, *Adv. Synth. Catal.*, 2014, **356**, 537–556.

15 (*a*) A. Padwa, *Chem. Soc. Rev.*, 2009, **38**, 3072–3081; (*b*) A. Domling, *Chem. Rev.*, 2006, **106**, 17–89; (*c*) D. M. D'Souza and T. J. J. Muller, *Chem. Soc. Rev.*, 2007, **36**, 1095–1108; (*d*) D. Tejedor and F. G. Tellado, *Chem. Soc. Rev.*, 2007, **36**, 484–491; (*e*) V. Polshettiwar and R. S. Varma, *Chem. Soc. Rev.*, 2008, **37**, 1546–1557.

16 C. Hulme and V. Gore, *Curr. Med. Chem.*, 2003, **10**, 51–80.

17 (*a*) C. J. O'Connor, H. S. G. Beckmann and D. R. Spring, *Chem. Soc. Rev.*, 2012, **41**, 4444–4456; (*b*) E. Ruijter, R. Scheffelaar and R. V. A. Orru, *Angew. Chem., Int. Ed.*, 2011, **50**, 6234–6246.

18 J. Elflein, *Pharma and Medtech*, 2021.

19 M. Marcovecchio, A. Mohn and F. Chiarelli, *J. Endocrinol. Invest.*, 2005, **28**, 853–863.

20 H. Rasouli, S. M. Hosseini-Ghazvini, H. Adibi and R. Khodarahmi, *Food Funct.*, 2017, **8**, 1942–1954.

21 J. R. N. Taylor, M. N. Emmambux and J. Kruger, *Starch-Starke*, 2015, **67**, 79–89.

22 P. M. Sales, P. M. Souza, L. A. Simenoni, P. O. Magalhaes and D. Sliveria, *J. Pharm. Pharm. Sci.*, 2012, **15**, 141–183.

23 Y. Tan, S. K. C. Chang and Y. Zhang, *Food Chem.*, 2017, **214**, 259–268.

24 W. Puls, U. Keup, H. Krause, P. G. Thomas and F. Hoffmeister, *Naturwissenschaften*, 1977, **64**, 536–537.

25 K. V. Dileep, K. Nithiyanandan and C. Remya, *J. Biomol. Struct. Dyn.*, 2018, **36**, 3354–3361.

26 O. J. Afonne, O. E. Orisakwe, E. Obi, C. Orish and D. D. Akumka, *Indian J. Pharmacol.*, 2000, **32**, 239–241.

27 P. Daisy, R. Jasmine, S. Ignacimuthu and E. Murugan, *J. Phytomed.*, 2009, **16**, 252–257.

28 A. Shirwaikar, K. Rajendran and I. S. R. Punitha, *J. Ethnopharmacol.*, 2005, **97**, 369–374.

29 O. Akerele, *World Health Forum*, 1993, **14**, 390–395.

30 R. Geethalakshmi, D. V. L. Sarada, P. Marimuthu and K. Ramasamy, *Int. J. Biotechnol. Biochem.*, 2010, **6**, 369–376.

31 S. Dewanjee, A. K. Das, R. Sahu and M. Gangopadhyay, *Food Chem. Toxicol.*, 2009, **47**, 2679–2685.

32 N. Nivetha and A. Thangamani, *J. Mol. Struct.*, 2021, **1242**, 130716.

33 L. D. Chiaradia, P. G. A. Martins, M. N. S. Cordeiro, R. V. C. Guido, G. Ecco, A. D. Andricopulo, R. A. Yunes, J. Vernal, R. J. Numes and H. Terenzi, *J. Med. Chem.*, 2012, **55**, 390–402.

34 C. E. P. Galvis and V. V. Kouznetsov, *Org. Biomol. Chem.*, 2013, **11**, 7372–7386.

35 (*a*) A. Dandia, A. K. Jain and D. S. Bhati, *Tetrahedron Lett.*, 2011, **52**, 5333–5337; (*b*) H. Liu, G. Dou and D. Shi, *J. Comb. Chem.*, 2010, **12**, 633–637.

36 R. Satheeshkumar, L. Edatt, V. B. S. Kumar and K. J. R. Prasad, *ChemistrySelect*, 2017, **2**, 2626–2633.